Microstructural evolution and deformation behavior in the Fe-(6, 8.5)Mn-3Al-0.2C TRIP steels

Z.C. Li[1,2], H. Ding[1]*, R.D.K. Misra[2]*, Z.H. Cai[1], H.X. Li[1]

[1] School of Materials Science and Engineering,
Northeastern University, Shenyang, 110819, China
[2] Laboratory for Excellence in Advanced Steel Research,
Department of Metallurgical, Materials and Biomedical Engineering,
University of Texas at El, Paso, El Paso, TX 79968, USA

Abstract

We have studied here the microstructural evolution and deformation behavior in two hot-rolled Fe-6Mn-3Al-0.2C (6Mn steel) and Fe-8.5Mn-3Al- 0.2C (8.5Mn steel) transformation induced plasticity (TRIP) steels. Excellent combination of mechanical properties including total elongation (TEL) of 39.3%, ultimate tensile strength (UTS) of 1112 MPa and UTS×TEL of 43.7 GPa% were obtained in 8.5Mn steel subjected to intercritical hardening at 750℃ and tempering at 200℃. The increase in the Mn-content in the experimental steel led to increase in the volume fraction of austenite and change in austenite morphology. Non-uniform Mn distribution in austenite with varied morphology resulted in different degree of austenite stability and led to discontinuous TRIP effect, contributing to the best combination of mechanical properties in 8.5Mn-750 steel.

Keywords: microstructural evolution; mechanical properties; deformation behavior; discontinuous TRIP effect; austenite morphology

---

*Corresponding author: E-mail: dinghuaneu@163.com (H. Ding); dmisra2@utep.edu (R.D.K. Misra).

1. Introduction

Transformation induced plasticity (TRIP) steels with high strength, superior ductility, and good crashworthiness are potential candidates for automotive applications [1]. The increased demand for energy conservation, environmental protection and reduced weight of automobiles has led to significant interest in the development of new advanced high strength steels. Medium Mn-content (5-12%) transformation-induced plasticity (TRIP) steels are potential candidates for automotive applications, where the TRIP effect can be completely utilized [2].

The product of ultimate tensile strength and total elongation (PSE) is considered an index of ability to absorb impact energy [3]. The conventional low-alloyed TRIP steels with Mn-content of $\leqslant$ 2.5% are characterized by PSE of ～15±10GPa%, and consist of several phases including ferrite (dominant phase), retained austenite, bainite, and occasionally a small amount of martensite [4-6].

Recently, studies [7-12] have been carried out on medium Mn (4-10%) steels that are considered promising automotive steels with PSE$\geqslant$30GPa%. It is proposed [10-11] that the stability of austenite can be attributed to significant partitioning of Mn between ferrite and austenite during long (hours) of holding time in the intercritical region. Miller [11] reported austenite fraction of up to 30% in 6.0% Mn alloys. More recently, Merwin [12] obtained retained austenite volume fraction up to 17% in 0.10C-5.2Mn alloy, 28% in 0.10C-5.8Mn alloy and 38% in 0.10C-7.1Mn alloy. Li et al. [13] reported austenite fraction of up to 33% in 0.20C-6Mn-3.2Al alloy. While, retained austenite volume fraction up to 65% in 0.20C-11Mn-3.8Al alloy was obtained by Cai et al. [14]. Thus, it was suggested that the mechanical properties, PSE in particular, is significantly improved with increased Mn-content, which leads to increased volume

fraction of retained austenite.

The objective of the study described here is to explore microstructural evolution, mechanical properties and deformation behavior of two hot-rolled steels with medium Mn-content, in the endeavor to understand the effect of Mn on austenite morphology, mechanical properties and deformation behavior.

2. Materials and experimental procedure

The nominal composition of the two experimental steels was 0.2C-3Al-6Mn-Fe (wt.%) (6Mn steel) and 0.2C-3Al-8.5Mn-Fe (wt.%) (8.5Mn steel). The chemical composition is listed in Table 1. Experimental steel ingots of 40 kg were cast after melting in a vacuum induction furnace. The ingots were heated at 1200℃ for 2 h, hot forged into rods of section size 100 mm ×30 mm, and air cooled to room temperature (RT). Subsequently, the rods were soaked at 1200℃ for 2 h, hot-rolled to 4 mm thick strip in the temperature range of 1150-850℃, and finally air cooled to room temperature (RT).

A model proposed by E. De Moor et al. [15] was used to predict the amount of austenite stabilized to room temperature through the enrichment of austenite with Mn, Al and C. It was further deduced that there existed a temperature in the intercritical region resulting in maximum austenite retention at room temperature. The model was instructive in optimizing the alloy design of experimental steels.

The phase transformation temperatures were determined by dilatometer experiments. The sample used for dilatometry was a solid cylindrical specimen with a length of 10 mm and diameter of 3 mm. After thermal expansion in the heating stage (20-1100℃) at the rate of 20℃/s,

the sample was held at 1100℃ for 3 min. As indicated in Table 1, the intercritical temperature range of 6Mn steel and 8.5Mn steel were 665-846℃ and 629-867℃, respectively.

A two-stage heat treatment which can stabilize austenite during annealing was adopted [16]. The medium-Mn steels were first soaked in the austenite region and quenched to obtain a fully martensitic structure. Next, an intercritical annealing followed by air cooling was adopted to stabilize a high fraction of retained austenite. The formation of austenite from the initial martensitic structure is referred as "austenite reverted transformation" (ART) [8-12]. However, this is not applicable to the experimental steels studied here. A long time annealing renders austenite too stable and weakens the TRIP effect. In our case, the as-hot-rolled sheets were subjected to Q&T heat treatment. First, they were annealed in the two-phase region for 1 h, followed by water quenching to room temperature. Second, the quenched samples were tempered at 200℃ for 20 min and then air cooled to room temperature. Tempering not only helps to relieve the internal stress, but also improves the stability of austenite [17].

Tensile specimens of dimensions 12.5 mm width and gage length of 50 mm were machined from the heat-treated sheets with the tensile axis parallel to the rolling direction. The tensile tests were carried out at room temperature using a universal testing machine (SANSCMT5000) at a constant crosshead speed of 3 $mm \cdot min^{-1}$. The samples were etched with 25% sodium bisulfite solution. Microstructural examination was carried out using scanning electron microscope (SEM). The volume fraction of austenite was determined by X-ray diffraction (XRD) with CuK_{α} radiation using direct comparison method [18].

3. Results and discussion

3.1 Composition design

The phase fractions of the two experimental steels based on an equilibrium thermodynamic analysis predicted by Thermo-Calc are presented in Figs. 1a and 1b and these predicted equilibrium austenite fractions were used as inputs to the model. Predictions of austenite composition were also made using Thermo-Calc and the predicted C, Mn, and Al-contents in austenite of 6Mn steel and 8.5Mn steel are presented in Figs. 1c and 1d, respectively. It is clear that C and Mn-content of austenite varied with temperature, while Al-content was insensitive to temperature. Thus, it can be inferred that C and Mn have significant impact on the stability of austenite, while Al does not appear to influence austenite stability. The predicted fraction of retained austenite in the two experimental steels as a function of annealing temperature is presented in Figs. 1e and 1f. For 6Mn steel, a pronounced peak (～38 vol.%) was observed at ～690℃ and for 8.5Mn steel, the maximum retained austenite fraction approached ～65 vol.% at ～755℃.

3.2 Microstructure

Fig. 2 shows the SEM microstructure of heat-treated 6Mn steel. As shown in Figs. 2a and 2b, the microstructural constituents in steels quenched from 650℃ and 700℃, respectively, followed by tempering at 200℃ consisted of intercritical ferrite (IF), δ-ferrite (δ-F) and austenite (A). With increase in annealing temperature, the volume fraction and grain size of austenite was increased and the volume fraction of ferrite was decreased during annealing in the intercritical region. The intercritical ferrite (IF) that formed during intercritical annealing had different morphology compared to the layered δ-ferrite. In the case of steels quenched from 750℃ and 800℃, respectively, the microstructural constituents were IF, δ-F, austenite and

martensite (M) (Figs. 2c and 2d). It is clear that austenite decreased because of martensitic transformation. The transformed martensite grew and became thicker with increased temperature.

Fig. 3 shows SEM micrographs of heat-treated 8.5Mn steel. The microstructural constituents of the steels quenched from 650℃, 700℃ and 750℃, respectively, followed by tempering at 200℃ consisted of intercritical ferrite (IF), δ-ferrite (δ-F) and austenite (A), as shown in Figs. 3a, 3b and 3c. The volume fraction of blocky austenite increased with increase in quenching temperature. For the steel quenched from 800℃, the microstructural constituents consisted of IF, δ-F, austenite and martensite (M) (Fig. 3d). The morphology of each phase varied significantly with different intercritical hardening temperatures.

The 8.5Mn steel contained relatively more austenite than 6Mn steel, whereas the amount of ferrite in 8.5Mn steel was less than in 6Mn steel. The volume fraction of austenite was determined by XRD using direct comparison method, involving use of integrated intensities of $(200)_\alpha$ and $(211)_\alpha$ peaks and those of $(200)_\gamma$, $(220)_\gamma$ and $(311)_\gamma$ peaks. The volume fraction of austenite V_A was calculated using equation (1) [19]:

$$V_A = 1.4I_\gamma / (I_\alpha + 1.4I_\gamma) \quad (1)$$

where I_γ is the integrated intensity of austenite and I_α is the integrated intensity of α-phase. The variation in volume fraction of austenite obtained from XRD is summarized in Fig. 4a. It is known that the volume fraction of austenite was increased and the volume fraction of ferrite was decreased with increase in annealing temperature during annealing in the intercritical region. Thus, it is clear that the austenite fraction of 8.5Mn steel increased from 22 vol.% to 58.5 vol.% with increase in temperature from 600℃ to 750℃, followed by a sharp decrease to 24 vol.%

when heat-treated at 800℃ because of martensitic transformation (Fig. 3d). Similar variation in austenite fraction was observed in 6Mn steel, consistent with the SEM micrographs (Fig. 2).

The transformation ratio of austenite in 6Mn steel and 8.5Mn steel are presented in Fig. 4b. A reduction in austenite grain size can effectively increase austenite stability by suppressing martensite transformation [20-23]. For 6Mn steel and 8.5Mn steel, the austenite grain size increased with increase in temperature. Moreover, according to the calculation results (Figs. 1c and 1d), Mn-content in austenite decreased with increase in temperature. A decrease in Mn content, which is strong austenite stabilizer, decreases the stability of austenite at room temperature [24]. An increase in austenite grain size also decreases austenite stability by facilitating martensitic transformation [25]. Thus, with increased temperature, the austenite stability decreased and austenite transformed to martensite more easily during tensile deformation. As a result, the transformation ratio of austenite increased with increase in temperature until the austenite transformed to martensite after quenching for 6Mn steel and 8.5Mn steel quenched from 750℃ and 800℃, respectively. Schematic diagrams of the volume fraction of ferrite, austenite and martensite in 6Mn steel and 8.5Mn steel heat-treated at different temperatures are presented in Fig. 5. During annealing in the intercritical region, the volume fraction of austenite was increased and the volume fraction of ferrite was decreased with increase in annealing temperature. Thus, when 6Mn steel and 8.5Mn steel were heat-treated in the temperature range of 650-700℃ and 600-750℃, respectively, the volume fraction of austenite increased with increase in temperature. Compared to 6Mn steel, 8.5Mn steel had higher volume fraction of austenite. With increase in temperature, the austenite stability decreases because of increase in austenite grain size. For 6Mn steel heat-treated in the temperature range of 750-850℃,

the higher temperature the more austenite transformed to martensite on quenching. For 8.5Mn steel heat-treated at 800℃, the volume fraction of austenite decreased because of martensitic transformation.

3.3 Mechanical properties

The mechanical properties are illustrated in Fig. 6. Figs. 6a and 6b show that ultimate tensile strength (UTS) of the two steels increased continuously with the increased temperature, whereas total elongation (TEL) of 6Mn steel and 8.5Mn steel decreased with increase in temperature after attaining the peak value of 35.4% at 700℃ (6Mn-700 steel) and 39.3% at 750℃ (8.5Mn-750 steel), respectively. As shown in Fig. 6c, when 6Mn steel and 8.5Mn steel were heat-treated at 700℃ and 750℃, respectively, the samples exhibited optimal mechanical properties. For 6Mn-700 steel, UTS of 942 MPa, TEL of 35.4%, and PSE of 33.3GPa% were obtained, while for 8.5Mn-750 steel, the properties were, UTS-1112 MPa, TEL-39.3%, and PSE-43.7GPa%. In contrast, other medium Mn TRIP steels had near similar strength with a lower or similar plasticity, but additional cold-rolling or prolonged annealing was required [7,9,11,26]. Therefore, the experimental steel samples had significantly superior tensile properties compared to those reported for medium Mn-content TRIP steels, as shown in Table 2 [14,27-28].

The flow stress of multiphase steel (σ_F) can be estimated using the rule of mixtures proposed by Embury and Bouaziz (equation (2)) [29-30],

$$\sigma_F = f_\alpha \sigma_\alpha + (f_\gamma - f_{nm})\,\sigma_\gamma + (f_m + f_{nm})\,\sigma_m \qquad (2)$$

where σ_α, σ_γ, σ_m are the flow stresses and f_α, f_γ, f_m, f_{nm} are the volume fractions of ferrite, austenite, martensite and newly generated martensite during tensile testing, respectively. In the case of

8.5Mn steel, when the samples were heat-treated in the range of 600-750℃, the microstructural constituents consisted of austenite and ferrite, based on XRD results, and the austenite fraction and the transformation ratio of austenite increased with increasing temperature (Fig. 4). Thus, σ_F is determined by the austenite fraction and TRIP effect. Meanwhile, TEL increased with increasing temperature and is attributed to TRIP effect. When sample was heat-treated at 800℃, the microstructural constituents consisted of ferrite, austenite, and martensite as the dominant phases. Such that σ_F depends on the fraction of martensite. Because of increasing martensite fraction, TEL decreases with the increasing temperature. The variation of UTS and TEL of 6Mn steel samples can be interpreted in a similar way.

A comparison between Figs. 4, 5 and 6 shows that TEL followed a similar trend with the volume fraction of austenite. Combining XRD results (Fig. 4a) and mechanical properties (Fig. 6), one interesting phenomena was observed. 8.5Mn-700 steel was comprised of 43 vol.% austenite. In contrast, 6Mn-700 steel comprised of 33.1 vol.% austenite. Interestingly, the corresponding TEL for 6Mn-700 steel was higher than 8.5Mn-700 steel (6Mn-700: 35.4%, 8.5Mn-700: 34.5%). The underlying reason for the phenomena can be elucidated by studying the deformation behavior and austenite stability.

3.4 Deformation behavior and Austenite Stability

Fig. 7 shows a comparison of X-ray diffraction pattern of 6Mn-700 and 8.5Mn-750 undeformed samples with the fractured samples. It is implied that the austenite fraction was reduced to a small amount after tensile failure. The volume fraction of retained austenite measured by XRD analysis for 6Mn-700 and 8.5Mn-750 fractured samples were 14.3 vol.% and 19.9 vol.%, respectively, and the original amount of austenite were 33.1 vol.% and 58.5 vol.%,

respectively. The transformation ratio of austenite in 6Mn-700 steel and 8.5Mn-750 steel was 56.8% and 66.0%, respectively (as shown in Fig. 4b). Thus, it indicates that significant TRIP effect took place during tensile deformation.

As shown in Fig. 8b, the work hardening behavior of 6Mn-700, 8.5Mn-700 and 8.5Mn-750 steels exhibited three stages of work hardening rate (WH) evolution: WH rapidly decreases in stage 1; then decreases slowly (stage 2) before finally decreasing rapidly (stage 3) with increasing tensile strain. According to the previous reports [8, 31], steels with 5-7% Mn content exhibited three domains of work hardening rate evolution: (1) work hardening rate (WH) rapid decreases; (2) re-enhancement of WH; (3) final smooth drop of WH. The three-step behavior is known to be related to the strain induced transformation of austenite into martensite (TRIP effect). Jie Shi et al. [8] ascribed the existence of three-stage WH to the samples having a retained austenite fraction higher than 15%. In majority of the studies [8, 31-33], the first stage is associated with the deformation of ferrite, the second intermediate stage characterized by a higher work hardening rate is related to the occurrence of TRIP effect, and the final stage is probably associated with deformation of ferrite and martensite because martensitic transformation is inactive in this stage.

Work hardening ability is expected to be influenced by austenite stability. In the attempt to quantify this behavior, equation (3) was used [34]:

$$k = - \ln(f_\gamma / f_{\gamma 0}) / \varepsilon \quad (3)$$

where $f_{\gamma 0}$, f_γ and k are the initial austenite fraction, the austenite fraction at strain ε and the mechanical stability of austenite, respectively. A higher value of k corresponds to lower austenite mechanical stability. For 8.5Mn-700 steel (k=2.6), the WH decreased more rapidly in stage 2 and

corresponds to a smaller strain region than 6Mn-700 steel (k=2.9). This implies relatively low TRIP effect and work hardening ability in 8.5Mn-700 steel, because of which the elongation was low. In the case of 8.5Mn-750 steel (k=3.3), the second intermediate stage characterized by an increase in work hardening rate is attributed to significant occurrence of TRIP effect. 8.5Mn-750 steel demonstrated highest work hardening ability and resulted from highest austenite fraction and k value. Interestingly, an obvious difference in stage 2 of 8.5Mn-750 steel was that it decreased with fluctuation, which is directly related to the observed serrations in the true stress-strain plot presented in Fig. 8a. The serrated behavior is attributed to the discontinuous TRIP effect involving stress relaxation and transfer during deformation with consequent enhancement in ductility, which was proposed by Cai et al. [35]. The discontinuous TRIP effect occurs at a critical stress during the deformation process, thereby invoking relaxation and transfer of local stress, and contributes to additional strain. Thus, in 6Mn-700 and 8.5Mn-700 steels, TRIP effect contributed to ductility. In contrast, the excellent mechanical properties of 8.5Mn-750 steel was primarily associated with the discontinuous TRIP effect, and the TRIP effect is mainly influenced by austenite stability rather than by the austenite fraction.

It was interesting to note that the discontinuous TRIP effect occurred in 8.5Mn-750 steel, but it did not appear in other samples. Recently, it was proposed by Cai et al. [35] that discontinuous TRIP effect primarily results from austenite with different degree of stability. Thus, it is worthwhile to find out the reason underlying the varying degree of austenite stability.

The 6Mn steel and 8.5Mn steel obtained the highest volume fraction of austenite on heat treatment at 700℃ and 750℃, respectively. Fig. 9 shows schematic illustrations of the austenite morphology in 6Mn-700 steel and 8.5Mn-750 steel. 8.5Mn-750 steel had higher volume fraction

of austenite than 6Mn-700 steel. In case of 6Mn-700 steel, the austenite was lath-like. In contrast, in 8.5Mn-750 steel, austenite consisted of blocky austenite and lath-like austenite and the grain size of austenite in 8.5Mn-750 steel varied.

Figs. 10a and 10b are the SEM micrographs of 6Mn-700 steel and the corresponding manganese partitioned in austenite. EDS was used to estimate the approximate partitioning of Mn. The microstructural constituents of austenite mainly consisted of lath-like austenite. The statistical results of ten randomly selected grain dots presented in Fig. 10b indicated that the Mn distribution in the austenite grains was uniform (Mn average: 7.1 wt.%). In 8.5Mn-750 steel, austenite was both blocky and lath-like, as shown in Fig. 10c. The statistical results of ten randomly selected grain dots presented in Fig. 10d indicated that the Mn distribution was higher in lath-like austenite (Mn average: 11.1 wt.%) than in blocky austenite (Mn average: 7.3 wt.%).

Based on the analysis above, it is implied that the increase in Mn-content in the experimental steel not only increased the volume fraction of austenite but also changed the austenite morphology. Moreover, the non-uniform distribution of Mn in austenite of different morphology resulted in different degree of austenite stability. It is clear that the stability of austenite in 8.5Mn-750 steel varied, while it was uniform in other samples, because of which serrated work-hardening behavior in stage 2 was only observed in 8.5Mn-750 steel and led to the discontinuous TRIP effect, with best combination of mechanical properties.

4. Conclusions

The microstructural evolution, mechanical properties and deformation behavior in the hot-rolled Fe-6, 8.5Mn-3Al-0.2C TRIP steels was studied in detail. The major findings of the study are as follows:

(1) The calculation results of the maximum austenite retention at room temperature based on the proposed model were consistent with the experimental results. The high content of Mn in 8.5Mn steel led to higher fraction of austenite as compared to 6Mn steel.

(2) The hot-rolled 8.5Mn-750 steel exhibited best combination of mechanical properties, and was characterized by excellent combination of TEL of 39.3%, UTS of 1112 MPa and UTS×TEL of 43.7 GPa%, which is significantly superior compared to previously studied steels with similar Mn-content in TRIP steels. The excellent mechanical properties of 8.5Mn-750 steel were largely associated with the discontinuous TRIP effect.

(3) The increase in Mn-content in the experimental steel increased the volume fraction of austenite and also changed the austenite morphology. Non-uniform Mn distribution in austenite with varied morphology led to different degree of austenite stability, because of which the discontinuous TRIP effect was only observed in 8.5Mn-750 steel.

Acknowledgements

The present study was financially supported by the National Natural Science Foundation of China (No: 51031001), National Science Foundation for Young Scientists of China (No: 51501035) and Chinese Postdoctoral Science Foundation (2015M580230). R.D.K.M. gratefully acknowledges support from University of Texas at El Paso, USA and by National Science Foundation, USA through Grant # Ms Xuey phone number is: 13840376317.DMR1458074.

References

[1] V. Mertinger, E. Nagy, F. Tranta, J. Sólyom, Mater. Sci. Eng. A 481-482 (2008) 718-722.

[2] S. Oliver, T.B. Jones, G. Fourlaris, Mater. Sci. Technol. 23 (2007) 423-431.

[3] K. Sugimoto, T. Iida, J. Sakaguchi, T.Kashima, ISIJ. 9 (2000) 902-908.

[4] J. Mahieu, J. Maki, B.C. De Cooman, Metall. Mater. Trans. A 33A (2002) 2573-2580.

[5] Q. Furnémont, M. Kempf, P.J. Jacques, M. Göken, F. Delannay, Mater. Sci. Eng. A 328 (2002) 26-32.

[6] L. Samek, D.E. Moor, J. Penning, B.C. De Cooman, Metall. Mater. Trans. A 37A (2006) 109-124.

[7] S. Lee, S. Lee, B.C. De Cooman, Scr. Mater. 65 (2011) 225-228.

[8] S. Jie, X.J. Sun, M.Q. Wang, W.J. Hui, H. Dong, W.Q. Cao, Scr. Mater. 63 (2010) 815-818.

[9] R. Zhang, W.Q. Cao, Z.J. Peng, J. Shi, H. Dong, C.X. Huang, Mater. Sci. Eng. A 583 (2013) 84-88.

[10] S. Lee, S. Lee, S.S. Kumar, K. Lee, B.C. De Cooman, Metall. Mater. Trans. A 42A (2011) 3638-3651.

[11] R.L. Miller, Metall. Trans. 3A (1972) 905-912.

[12] P.J. Gibbs, E. De Moor, M. J. Merwin, B. Clausen, J.G. Speer, D.K. Matlock, Metall. Mater. Trans. A 42A (2011) 3691-3702.

[13] Z.C. Li, H. Ding, Z.H. Cai, Mater. Sci. Eng. A 639 (2015) 559-566.

[14] Z.H. Cai, H. Ding, X. Xue, Q.B. Xin, Mater. Sci. Eng. A 560 (2013) 388-395.

[15] E. De Moor, D.K. Matlock, J.G. Speer, M.J. Merwin, Austenite stabilization through manganese enrichment, Scr. Mater. 64 (2011) 185-188.

[16] D.D. Tjahjanto, A.S.J. Suiker, S. Turteltaub, Comput. Mater. Sci. 41 (2007) 107-116.

[17] Z.H. Cai, H. Ding, R.D.K. Misra, H. Kong, H.Y. Wu, Mater. Sci. Eng. A 595 (2014) 86-91.

[18] A.K. Srivastava, D. Bhattacharjee, G. Jha, N. Gope, S.B. Singh, Mater. Sci. Eng. A 445-446 (2007) 549-557.

[19] B.K. Jha, R. Avtar, V. Sagar Dwivedi, Trans. Ind. Inst. Met. 49(3) (1996) 133-142.

[20] R.D.K. Misra, V.S.A. Challa, P.K.C. Venkatsurya, Y.F. Shen, M.C. Somani, L.P. Karjalainen, Acta Mater. 84 (2015) 339-348.

[21] R.D.K. Misra, X.L. Wan, V.S.A. Challa, M.C. Somani, L.E. Murr, Mater. Sci. Eng. A 626 (2015) 41-50.

[22] V.S.A. Challa, X.L. Wan, M.C. Somani, L.P. Karjalainen, R.D.K. Misra, Scr. Mater. 86 (2014) 60-63.

[23] R.D.K. Misra, P.K.C. Venkatsurya, M.C. Somani, L.P. Karjalainen, Metall. Mater. Trans. A 43A (2012) 5286-5297.

[24] S.J. Lee, S. Lee, B.C. De Cooman, Scr. Mater. 64 (2011) 649-652.

[25] S.J. Lee, Y.K. Lee, Mater. Sci. Forum 475-479 (2005) 3169-3174.

[26] J.L. Zhao, Y. Xi, W. Shi, L. Li, J. Iron. Steel. Res. Int. 19(4) (2012) 57-62.

[27] M.J. Merwin, Mater. Sci. Forum. 539-543 (2007) 4327-4332.

[28] D.W. Suh, S.J. Park, T.H. Lee, Metall. Mater. Trans. A 41A (2010) 397-408.

[29] O. Bouaziz, Y. Bréchet, J. D. Embury, Advan. Eng. Mater. 10 (2008) 24-36.

[30] D. Embury, O. Bouaziz, Annu. Rev. Mater. Res. 40 (2010) 213-241.
[31] A. Arlazarov, M. Gouné, O. Bouaziz, A. Hazotte, G. Petitgand, P. Barges, Mater. Sci. Eng. A 542 (2012) 31-39.
[32] W.J. Dan, S.H. Li, W.G. Zhang, Z.Q. Lin, Mater. Design. 29 (2008) 601-612.
[33] B. K. Jha, R. Avtar, V.S. Dwivedi, V. Ramaswamy, J. Mater. Sci. Lett. 6 (1987) 891-893.
[34] K. Sugimoto, M. Kobayashi, S. Hashimoto, Metall. Mater. Trans. A 23A (1992) 3085-3091.
[35] Z.H. Cai, H. Ding, R.D.K. Misra, H. Kong, Scr. Mater. 71 (2014) 5-8.

Figure captions:

Fig. 1. Schematic illustration of the predictive model development for austenite stabilization as a function of temperature for 6Mn steel and 8.5Mn steel. (a)-(b) phase fractions, (c)-(d) C, Al and Mn-content in austenite and (e)-(f) calculated retained austenite fractions.

Fig. 2. SEM micrographs of hot-rolled 6Mn steels after quenching from different temperatures. (a) 650℃, (b) 700℃, (c) 750℃ and (d) 800℃.

Fig. 3. SEM micrographs of hot-rolled 8.5Mn steels after quenching from different temperatures. (a) 650℃, (b) 700℃, (c) 750℃ and (d) 800℃.

Fig. 4. Measured austenite fraction in undeformed and fractured samples and the transformation ratio of austenite in 6Mn steel and 8.5Mn steel heat-treated at different temperatures. (a) austenite fraction in undeformed and fractured samples of 6Mn steel and 8.5Mn steel and (b) transformation ratio of austenite in 6Mn steel and 8.5Mn steel.

Fig. 5. Schematic diagrams of the volume fraction of ferrite, austenite and martensite in (a) 6Mn steel and (b) 8.5Mn steel heat-treated at different temperatures.

Fig. 6. Comparisons of tensile properties between 6Mn steel and 8.5Mn steel. (a) UTS and TEL of 6Mn steel, (b) UTS and TEL of 8.5Mn steel and (c) UTS × TEL comparisons between 6Mn steel and 8.5Mn steel. (UTS-ultimate tensile strength, TEL-total elongation)

Fig. 7. XRD patterns of the undeformed and fractured samples. (a) 6Mn-700 samples and (b) 8.5Mn-750 samples.

Fig. 8. True stress-strain curves and work hardening rate of 6Mn-700, 8.5Mn-700 and 8.5Mn-750 steels. (a) True stress-strain curves and (b) work hardening rate.

Fig. 9. Schematic diagrams showing the morphology of austenite in the microstructure of (a) 6Mn-700 and (b) 8.5Mn-750 steels. The blue phase shows austenite phase and the white phase shows ferrite phase.

Fig. 10. SEM micrograph of 6Mn-700 and 8.5Mn-750 steels and the corresponding manganese partitioned in austenite by EDS. (a) SEM micrograph of 6Mn-700 steel, (b) Mn distribution in austenite of 6Mn-700 steel by EDS, (c) SEM micrograph of 8.5Mn-750 steel and (d) Mn distribution in blocky austenite and lath-like austenite of 8.5Mn-750 steel by EDS.

Tables:

Table 1. Chemical composition (wt.%) of steel and critical temperatures (℃).

Table 2. Comparisons of other medium Mn TRIP steels and experimental steels.

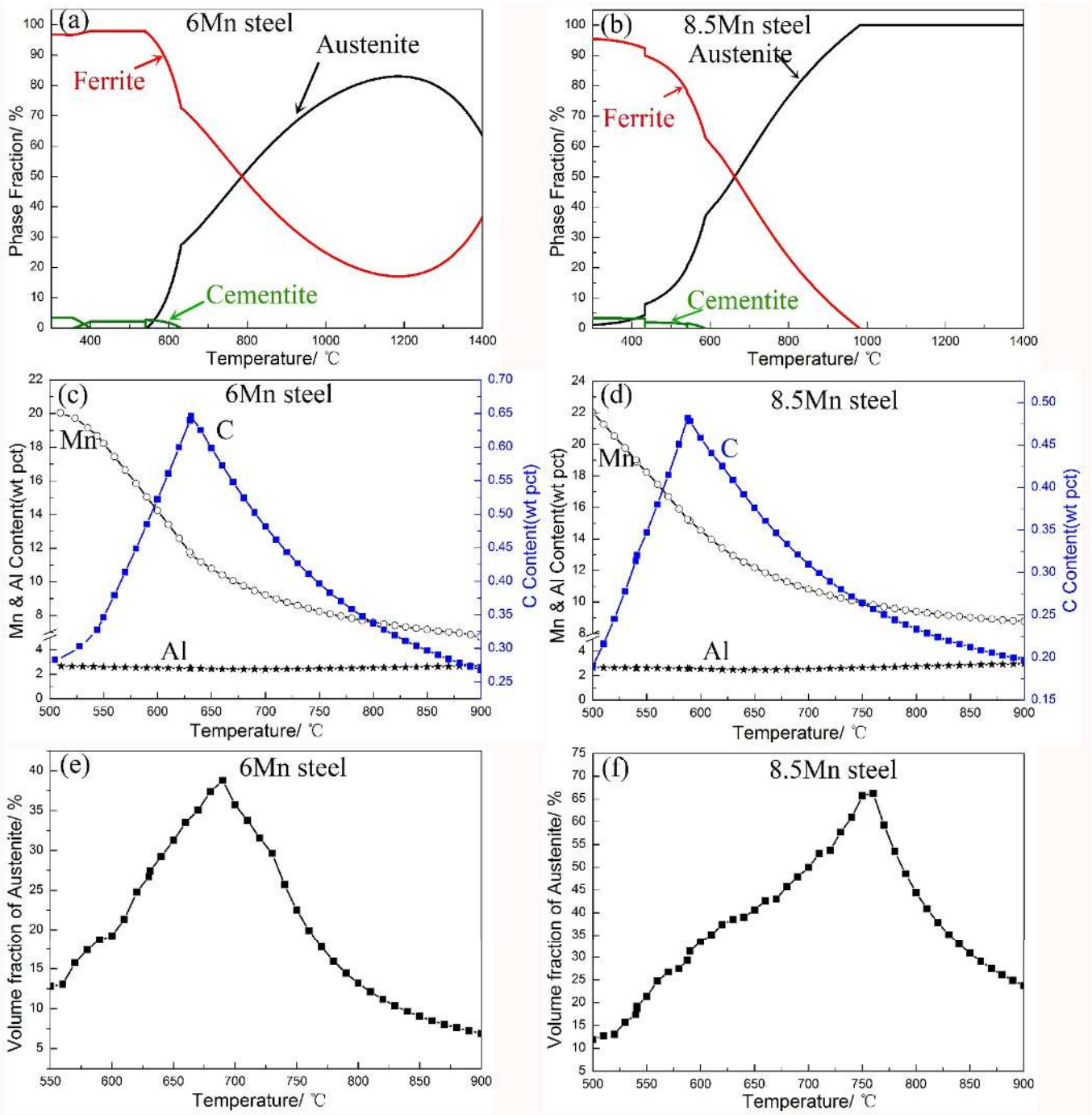

Fig. 1. Schematic illustration of the predictive model development for austenite stabilization as a function of temperature for 6Mn steel and 8.5Mn steel. (a)-(b) phase fractions, (c)-(d) C, Al and Mn-content in austenite and (e)-(f) calculated retained austenite fraction.

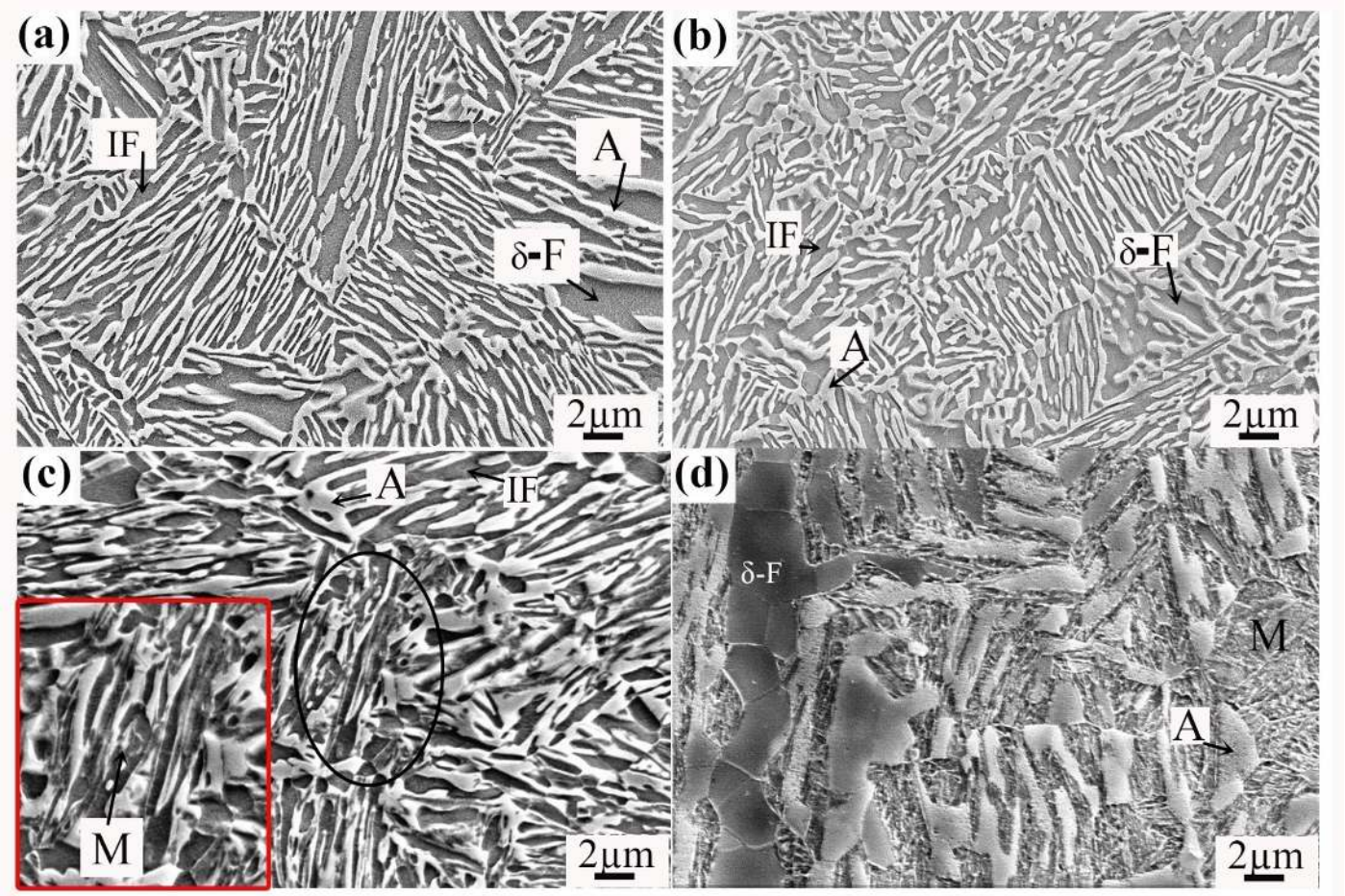

Fig. 2. SEM micrographs of hot-rolled 6Mn steels after quenching from different temperatures. (a) 650℃, (b) 700℃, (c) 750℃ and (d) 800℃.

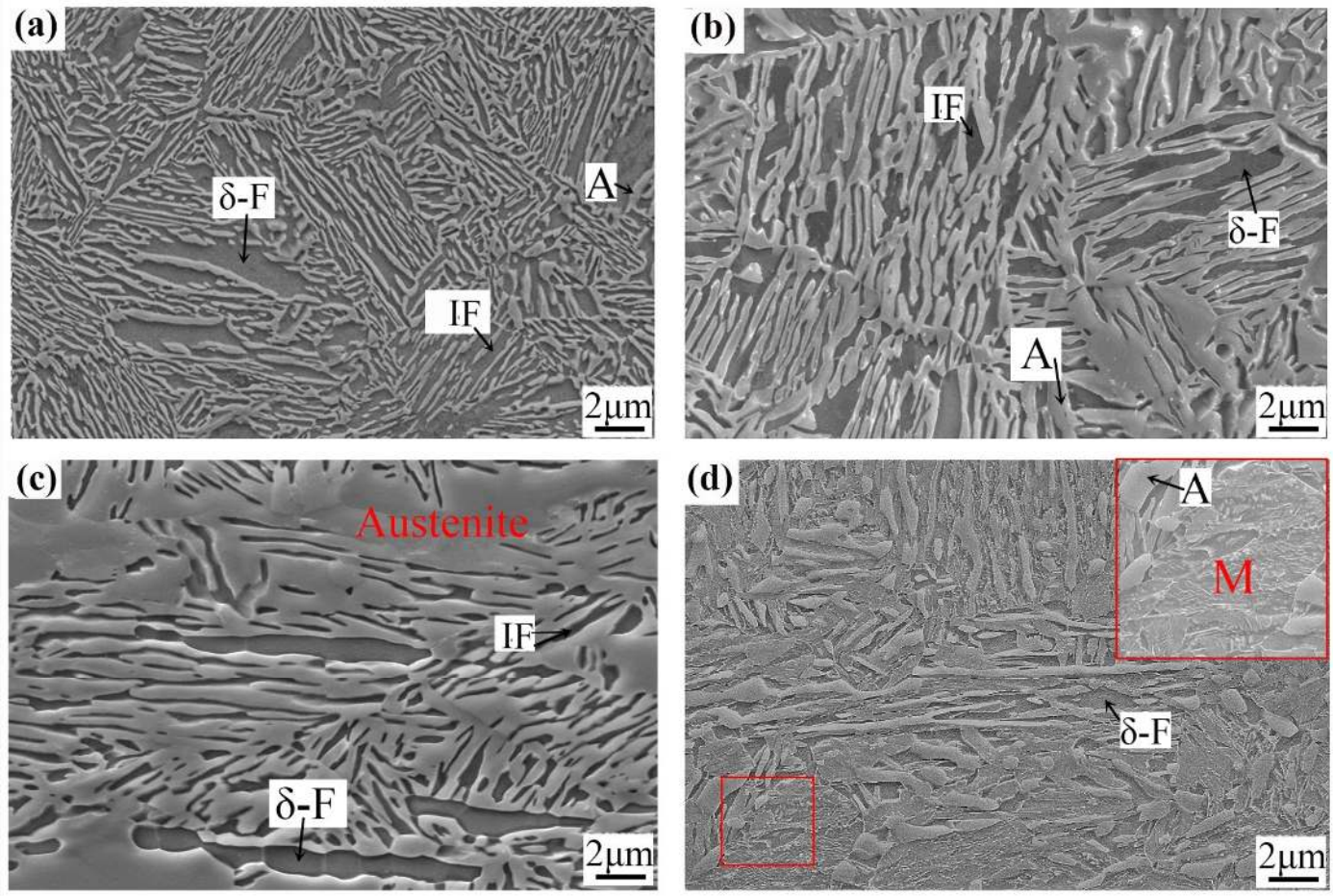

Fig. 3. SEM micrographs of hot-rolled 8.5Mn steels after quenching from different temperatures. (a) 650℃, (b) 700℃, (c) 750℃ and (d) 800℃.

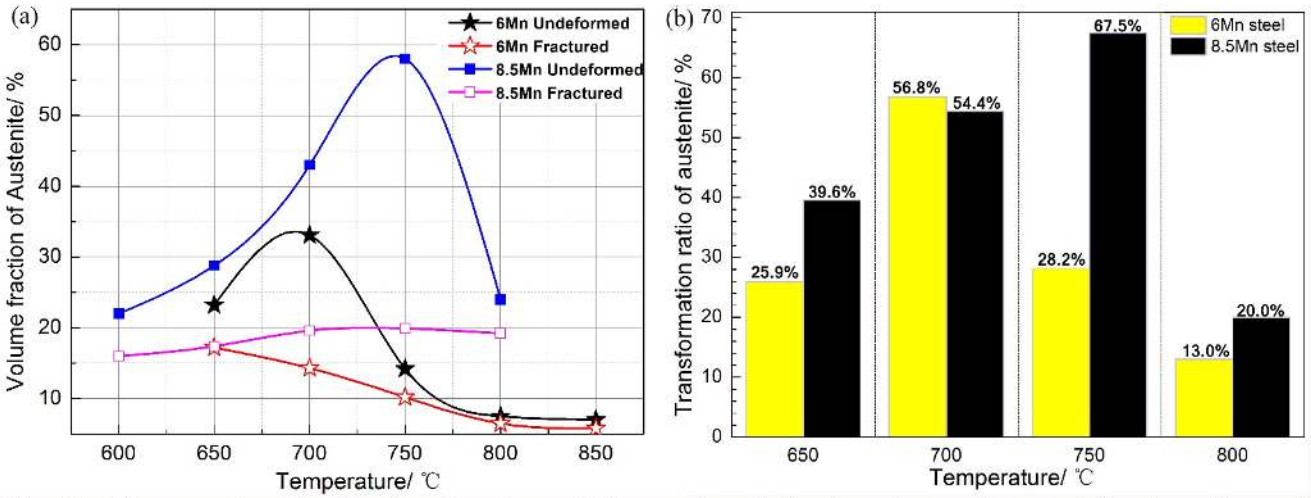

Fig. 4. Measured austenite fraction in undeformed and fractured samples and the transformation ratio of austenite in 6Mn steel and 8.5Mn steel heat-treated at different temperatures. (a) austenite fraction in undeformed and fractured samples of 6Mn steel and 8.5Mn steel and (b) transformation ratio of austenite in 6Mn steel and 8.5Mn steel.

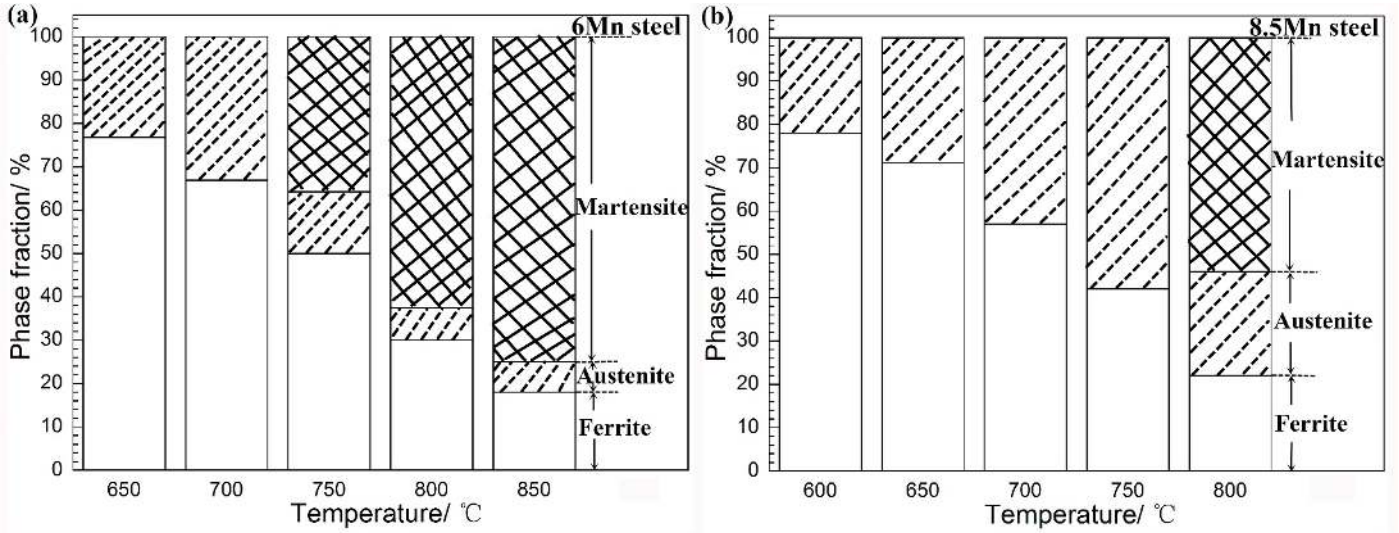

Fig. 5. Schematic diagrams of the volume fraction of ferrite, austenite and martensite in (a) 6Mn steel and (b) 8.5Mn steel heat-treated at different temperatures.

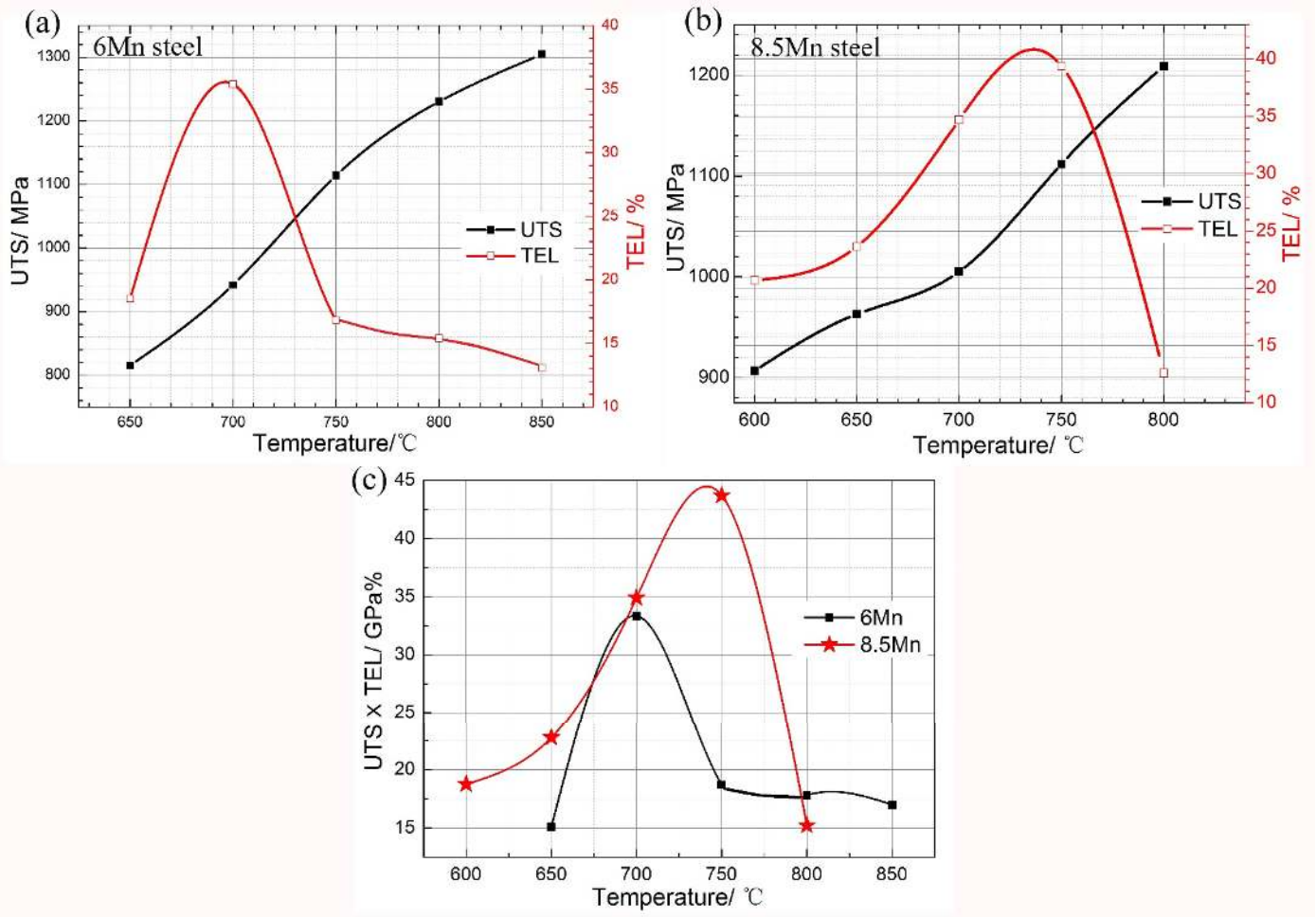

Fig. 6. Comparisons of tensile properties between 6Mn steel and 8.5Mn steel. (a) UTS and TEL of 6Mn steel, (b) UTS and TEL of 8.5Mn steel and (c) UTS × TEL comparisons between 6Mn steel and 8.5Mn steel. (UTS-ultimate tensile strength, TEL-total elongation)

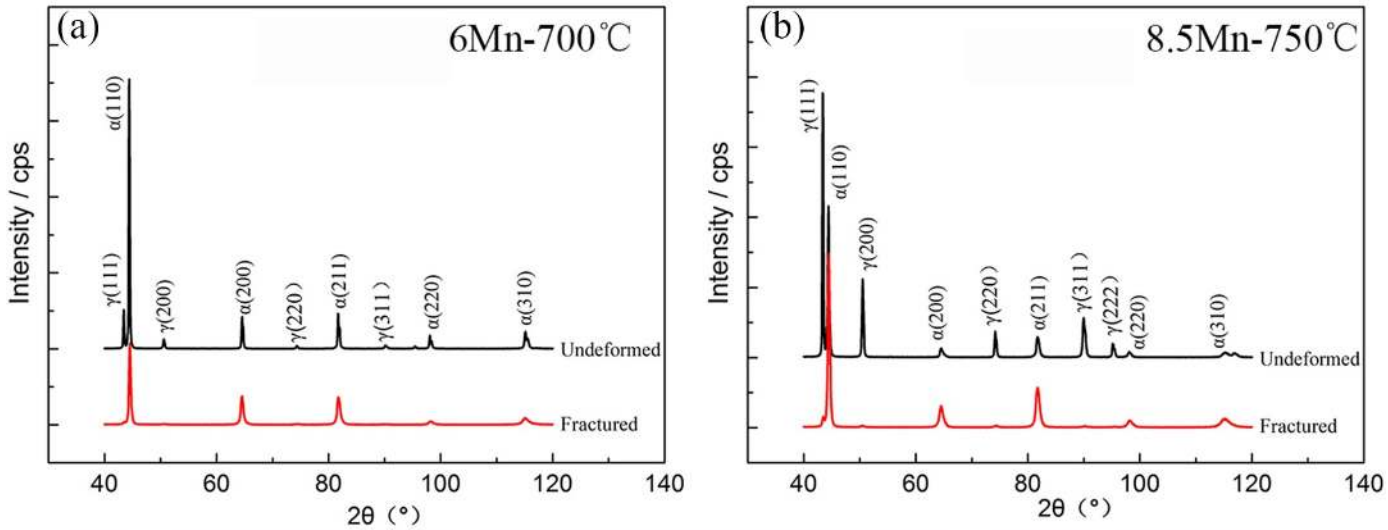

Fig. 7. XRD patterns of the undeformed and fractured samples. (a) 6Mn-700 samples and (b) 8.5Mn-750 samples.

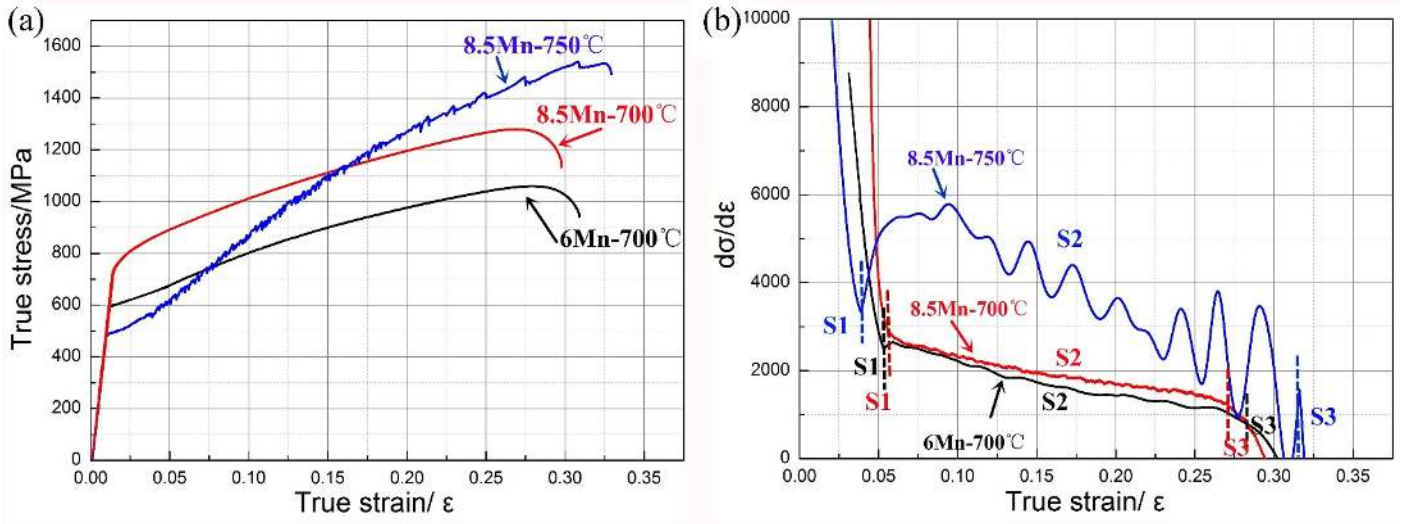

Fig. 8. True stress-strain curves and work hardening rate of 6Mn-700, 8.5Mn-700 and 8.5Mn-750 steels. (a) True stress-strain curves and (b) work hardening rate.

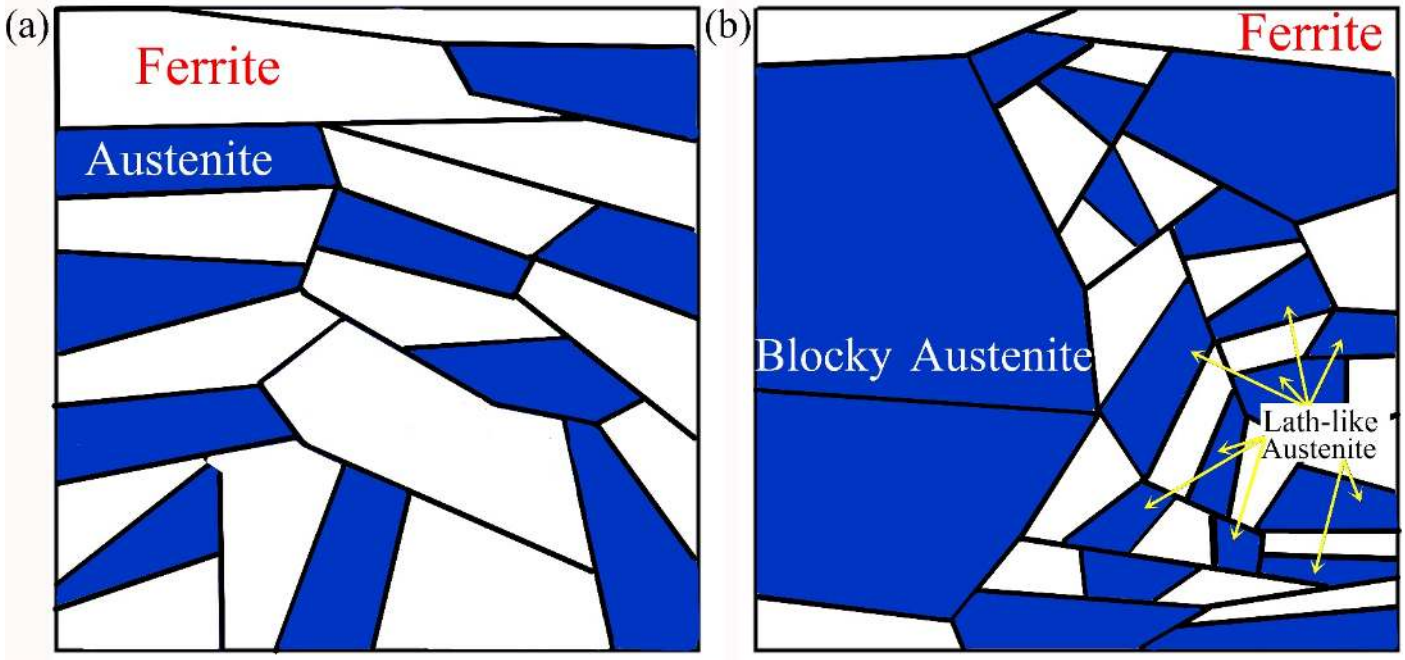

Fig. 9. Schematic diagrams showing the morphology of austenite in the microstructure of (a) 6Mn-700 and (b) 8.5Mn-750 steels. The blue phase shows austenite phase and the white phase shows ferrite phase.

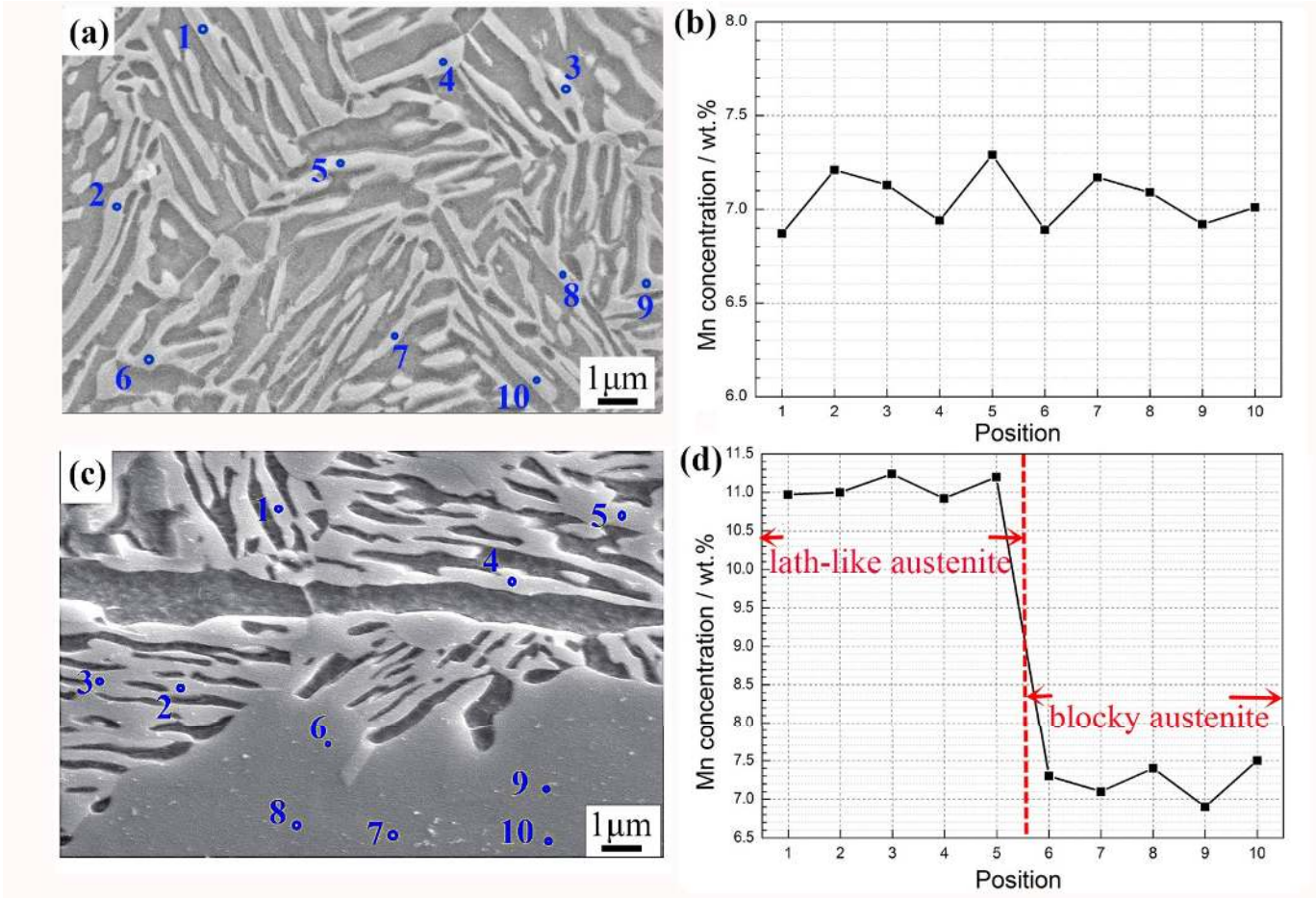

Fig. 10. SEM micrograph of 6Mn-700 and 8.5Mn-750 steels and the corresponding manganese partitioned in austenite by EDS. (a) SEM micrograph of 6Mn-700 steel, (b) Mn distribution in austenite of 6Mn-700 steel by EDS, (c) SEM micrograph of 8.5Mn-750 steel and (d) Mn distribution in blocky austenite and lath-like austenite of 8.5Mn-750 steel by EDS.

Table 1. Chemical composition (wt.%) of steel and critical temperatures (℃).

Steels	Mn	Al	C	Fe	Ac_1	Ac_3
6Mn	5.9	3.2	0.19	Bal	665	846
8.5Mn	8.37	3.11	0.19	Bal	629	867

Table 2. Comparisons of other medium Mn TRIP steels and experimental steels.

Composition	Initial condition	UTS(MPa)	TEL(%)	PSE(GPa%)	Reference
0.13C-6Mn-0.5Si-3.1Al	CR-annealing	854/1161	21.7/12.4	18.5/14.4	28
0.1C-7.1Mn	HR-annealing(80h)	1074	33.6	36.1	27
0.1C-7Mn	CR-annealing	1018	32	32.5	27
0.2C-11Mn-4Al	HR-QT(1h)	1082/1201	19.8/34.6	23.8/37.5	14
0.2C-6Mn-3Al	HR-QT(1h)	942	35.4	33.3	present work
0.2C-8.5Mn-3Al	HR-QT(1h)	1112	39.3	43.7	present work

CR-cold rolled steel, HR-hot rolled steel, QT-quenching and tempering, UTS-ultimate tensile strength, TEL-total elongation, PSE-product of strength and elongation.